The Astrophysical Journal, 650:261–271, 2006 October 10

THE AFTERGLOW, ENERGETICS, AND HOST GALAXY OF THE SHORT-HARD GAMMA-RAY BURST 051221a

A. M. Soderberg,[1] E. Berger,[2,3,4] M. Kasliwal,[1] D. A. Frail,[5] P. A. Price,[6] B. P. Schmidt,[7] S. R. Kulkarni,[1] D. B. Fox,[8] S. B. Cenko,[9] A. Gal-Yam,[1,4] E. Nakar,[10] and K. C. Roth[11]

Received 2006 January 20; accepted 2006 June 2

ABSTRACT

We present detailed optical, X-ray, and radio observations of the bright afterglow of the short gamma-ray burst 051221a obtained with Gemini, *Swift* XRT, and the Very Large Array, as well as optical spectra from which we measure the redshift of the burst, $z = 0.5464$. At this redshift the isotropic-equivalent prompt energy release was about 1.5×10^{51} ergs, and using a standard afterglow synchrotron model, we find that the blast wave kinetic energy is similar, $E_{K,\rm iso} \approx 8.4 \times 10^{51}$ ergs. An observed jet break at $t \approx 5$ days indicates that the opening angle is $\theta_j \approx 7^\circ$ and the total beaming-corrected energy is therefore $\approx 2.5 \times 10^{49}$ ergs, comparable to the values inferred for previous short GRBs. We further show that the burst experienced an episode of energy injection by a factor of 3.4 between $t = 1.4$ and 3.4 hr, which was accompanied by reverse shock emission in the radio band. This result provides continued evidence that the central engines of short GRBs may be active significantly longer than the duration of the burst and/or produce a wide range of Lorentz factors. Finally, we show that the host galaxy is actively forming stars at a rate of about 1.6 $M_\odot$ yr^{-1}, yet exhibits evidence for an appreciable population of old stars ($\sim$1 Gyr) and near-solar metallicity. These properties are intermediate between those of long GRB hosts and previous short burst hosts. The lack of bright supernova emission and the low circumburst density ($n \sim 10^{-3}$ cm^{-3}), however, continue to support the idea that short bursts are not related to massive stellar death. Given that the total energy release is larger than the predicted yield for a neutrino annihilation mechanism, this suggests that magnetohydrodynamic processes may be required to power the burst.

Subject heading: gamma rays: bursts

1. INTRODUCTION

Following over a decade of speculation about the nature of the short-duration hard-spectrum gamma-ray bursts (GRBs), the recent discovery of afterglow emission from these bursts provided the first physical constraints on possible progenitor models. We now know that short GRBs occur at cosmological distances, $z \gtrsim 0.1$, have energy releases of about 10^{49} ergs when corrected for relatively wide opening angles of $\sim 10^\circ$, are associated with both star-forming and elliptical galaxies, and are not associated with bright supernovae (Barthelmy et al. 2005; Berger et al. 2005; Bloom et al. 2006; Fox et al. 2005; Gehrels et al. 2005; Hjorth et al. 2005a, 2005b; Villasenor et al. 2005). These properties indicate that short GRBs are associated with an old stellar population, and are broadly consistent with expectations of the popular neutron star (NS) and/or black hole (BH) coalescence models (e.g., Eichler et al. 1989; Narayan et al. 1992; Katz & Canel 1996; Rosswog & Ramirez-Ruiz 2002; Aloy et al. 2005).

On the other hand, some of the afterglow observations, in particular the detection of soft X-ray tails and X-ray flares on a timescale $\gtrsim 10^2$ s (Barthelmy et al. 2005; Villasenor et al. 2005), cannot be easily explained in the coalescence scenario. These observations raise the possibility that short GRBs may have different or multiple progenitor systems (e.g., accretion-induced collapse of a neutron star; MacFadyen et al. 2005), or that some key physical processes in the energy-extraction mechanism or accretion disk hydrodynamics remain unaccounted for in the simple models (Perna et al. 2006). Secondary indicators such as the redshift and luminosity distributions have also been used to argue against the coalescence model (Nakar et al. 2006; but see Guetta & Piran 2005), but these rely on a very limited sample of events ($\lesssim 4$ with reasonably robust redshifts), and strong constraints are likely premature.

In the absence of direct evidence for or against the coalescence model, from the detection of either gravitational waves (e.g., Cutler & Thorne 2002) or a mildly relativistic outflow (Li & Paczyński 1998; Kulkarni 2005), progress in our understanding of the nature and diversity of the progenitor systems and the underlying physics requires a much larger statistical sample than the current data set of two short GRBs with secure redshifts (050709 and 050724) and two with putative redshifts (050509b and 050813). In addition, only GRBs 050709 and 050724 have broadband afterglow coverage, which allowed a determination of the energy release and circumburst density and provided evidence for ejecta collimation (Berger et al. 2005; Fox et al. 2005; Panaitescu 2006). With a larger sample of well-studied short GRBs

[1] Division of Physics, Mathematics and Astronomy, 105-24, California Institute of Technology, Pasadena, CA 91125.
[2] Observatories of the Carnegie Institution of Washington, 813 Santa Barbara Street, Pasadena, CA 91101.
[3] Princeton University Observatory, Peyton Hall, Ivy Lane, Princeton, NJ 08544.
[4] Hubble Fellow.
[5] National Radio Astronomy Observatory, Socorro, NM 87801.
[6] Institute for Astronomy, University of Hawaii, 2680 Woodlawn Drive, Honolulu, HI 96822.
[7] Research School of Astronomy and Astrophysics, Australian National University, Mount Stromlo Observatory, via Cotter Road, Weston Creek, ACT 2611, Australia.
[8] Department of Astronomy and Astrophysics, Pennsylvania State University, 525 Davey Laboratory, University Park, PA 16802.
[9] Space Radiation Laboratory, MS 220-47, California Institute of Technology, Pasadena, CA 91125.
[10] Theoretical Astrophysics, 130-33 California Institute of Technology, Pasadena, CA 91125.
[11] Gemini Observatory, 670 N. Aohoku Place Hilo, HI 96720.

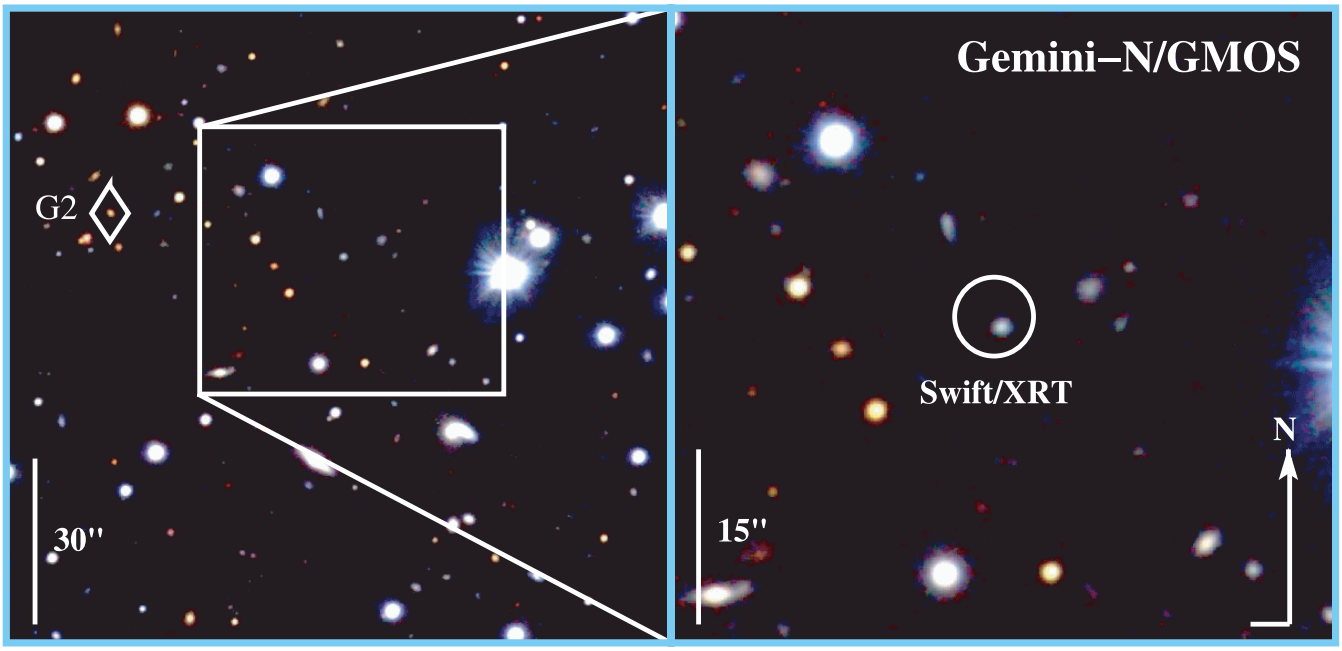

FIG. 1.—Color composite image of the field of GRB 051221a as observed with Gemini-N GMOS. The image is composed of i'- and z'-band data from 2005 December 27.2 UT and r'-band data from 2005 December 30.2 UT. The host galaxy of GRB 051221a is the only source detected inside the XRT error circle and is clearly blue as expected for a star-forming galaxy. We note that our spectrum of GRB 051221a also included galaxy G2 (*diamond*, *left panel*). This galaxy exhibits a strong Balmer/4000 Å break in addition to Ca II H and K absorption at $z = 0.849$. The presence of several nearby galaxies with a similar color and brightness may point to a background cluster unassociated with the burst.

we can begin to address the properties of the progenitor systems and the GRB mechanism through a census of the energy release, the jet opening angles, the density of the circumburst environment, and the relative fraction of short GRBs in star-forming and elliptical galaxies.

In this vein, we present in this paper detailed optical, X-ray, and radio observations of the bright GRB 051221a, which we localize to a star-forming galaxy at $z = 0.5464$. We show, from the evolution of the various light curves and from modeling of the broadband afterglow data, that the beaming-corrected energy release of this burst is comparable to those of previous short-hard bursts. In addition, we find that the circumburst density is low, indicating that the progenitor system is unlikely to reside in a star-forming region. Finally, we show that the GRB experienced an episode of significant energy injection, which was accompanied by reverse shock emission in the radio band. This, along with an energy release exceeding 10^{49} ergs, suggests that the energy extraction mechanism leads to a complex ejecta structure and is possibly driven by MHD processes rather than neutrino-antineutrino annihilation.

2. OBSERVATIONS

GRB 051221a was discovered by the *Swift* Burst Alert Telescope (BAT) on 2005 December 21.0773 UT (Parsons et al. 2005) and localized to a 0.′8 radius error circle centered on $\alpha = 21^{\rm h}54^{\rm m}50\overset{\rm s}{.}7$, $\delta = 16^\circ 53' 31\overset{''}{.}9$ (J2000.0; Cummings et al. 2005). The burst was also observed by the *Suzaku* Wideband All-sky Monitor (WAM; Endo et al. 2005) and by Konus-*Wind* (Golenetskii et al. 2005). The gamma-ray light curve is characterized by an initial hard pulse (FWHM ~0.25 s) composed of several separate pulses (FWHM ~15 ms) followed by a softer emission component lasting ~1 s (Norris et al. 2005; Endo et al. 2005; Golenetskii et al. 2005). The total duration of the burst is $T_{90} \approx 1.4 \pm 0.2$ s with a peak energy, $E_p \approx 400 \pm 80$ keV (Cummings et al. 2005; Golenetskii et al. 2005). The short duration and high E_p indicate that GRB 051221a is a classical short burst. The Konus-*Wind* gamma-ray fluence is $F_\gamma = 3.2^{+0.1}_{-1.7} \times 10^{-6}$ ergs cm^{-2} (20 keV–2 MeV; Golenetskii et al. 2005).

Starting at $t \approx 92$ s, the X-ray Telescope (XRT) on board *Swift* detected a fading source at $\alpha = 21^{\rm h}54^{\rm m}48\overset{\rm s}{.}71$, $\delta = 16^\circ 53' 28\overset{''}{.}2$ (J2000.0) with a 90% containment error radius of 3.″5 (Burrows et al. 2006). A near-infrared (NIR) object was identified within the XRT error circle, although it showed no evidence for fading between $t \approx 1.19$ and 1.38 hr after the burst (Bloom 2005a, 2005b).

2.1. *Optical Observations*

We began observations of GRB 051221a in the r' band using the Gemini Multi-Object Spectrograph (GMOS) on the Gemini-North 8 m telescope about 2.8 hr after the burst and detected a bright optical source coincident with the NIR object (Fig. 1). A comparison of the first and last exposures in the observation (227 and 271 minutes after the burst) revealed that the source has faded, indicating that it is the optical afterglow of GRB 051221a. Astrometry was performed relative to USNO-B using 60 sources in common between our summed image and the catalog, resulting in an rms positional uncertainty of 0.″18 in each coordinate. The position of the afterglow is $\alpha = 21^{\rm h}54^{\rm m}48\overset{\rm s}{.}63$, $\delta = +16^\circ 53' 27\overset{''}{.}4$ (J2000.0).

We continued to monitor the afterglow in the r', i', and z' bands for a period of about 9 days. A log of all Gemini observations is provided in Table 1. All observations were reduced using the standard `gmos` package in IRAF.

To study the afterglow variability and remove the contribution from the bright host galaxy, we used the ISIS subtraction routine by Alard (2000) which accounts for temporal variations in the stellar point-spread function (PSF). Adopting the final epoch observations in each filter as templates, we produced residual

TABLE 1
GEMINI-N GMOS OBSERVATIONS OF GRB 051221a

Date Obs (UT)	Δt (days)	Filter	Magnitude[a] (AB)
2005 Dec 21.2060	0.1287	r'	20.99 ± 0.08
2005 Dec 21.2194	0.1421	r'	21.07 ± 0.08
2005 Dec 22.2000	1.1227	r'	23.04 ± 0.08
2005 Dec 22.2114	1.1341	i'	23.11 ± 0.23
2005 Dec 23.2014	2.1241	i'	24.22 ± 0.35
2005 Dec 23.2150	2.1377	z'	23.92 ± 0.40
2005 Dec 23.2280	2.1515	r'	24.14 ± 0.12
2005 Dec 24.2020	3.1247	i'	< 23.99
2005 Dec 24.2158	3.1385	z'	< 23.98
2005 Dec 24.2294	3.1530	r'	24.12 ± 0.28
2005 Dec 26.2013	5.1240	i'	< 24.50
2005 Dec 26.2150	5.1377	z'	< 24.13
2005 Dec 26.2280	5.1518	r'	24.81 ± 0.21
2005 Dec 27.2030	6.1257	i'	...
2005 Dec 27.2194	6.1421	z'	...
2005 Dec 27.2358	6.1577	r'	< 24.74
2005 Dec 29.2046	8.1273	r'	< 24.92
2005 Dec 30.2042	9.1269	r'	...

[a] Photometry of residual images (see § 2.1). We have assumed the source flux to be negligible in the final (template) epoch for each filter. Errors are given as 1 σ and limits are given as 5 σ. These measurements are not corrected for Galactic extinction of $A_{r'} = 0.19$, $A_{i'} = 0.14$, and $A_{z'} = 0.12$ mag (Schlegel et al. 1998).

images (Fig. 2). Photometry was performed on the afterglow emission in each residual image. To estimate the error introduced by the subtraction procedure, we used IRAF `mkobject` to insert fake stars of brightness comparable to the afterglow at random positions on each image. The images were then subtracted and the false stellar residuals were photometered in the same manner as the afterglow residual. We adopt the standard deviation of the false residual magnitudes as an estimate for the error introduced by the subtraction procedure. This error is negligible for all observations before $t \sim 3$ days and is about 0.2 mag for subsequent observations.

For the later epochs in which the afterglow is not detected in our residual images, we estimate our detection threshold by performing photometry in blank apertures placed at random positions in the residual images. We use the standard deviation of the resulting photometry to estimate the limit (5 σ) to which we could reliably recover faint sources.

Field calibration was performed for the r'-band images using a GMOS observation of the standard star SA 92-250 in photometric conditions on 2005 December 30 UT. To calibrate the i' (z') band fields we used 23 (26) isolated, unsaturated stars in common with the USNO-B catalog and converted them to the SDSS photometric system according to the prescription of Smith et al. (2002). The photometric uncertainty in this calibration is 0.20 and 0.40 mag, respectively. We repeated this exercise for the r' band to further assess the accuracy of the USNO-B calibrations and find a zero point consistent to $\sim$0.20 mag with the standard star calibration. We estimate our total uncertainty for the afterglow observations by combining (in quadrature) the errors associated with the field calibration, subtraction procedure and photometric measurement (Table 1).

As shown in Table 1 and Figure 3, the afterglow is clearly detected in our r'-band images between $t \sim 0.1$ and 5.1 days after the burst. In the first image we find the afterglow to be $r' = 20.99 \pm 0.08$ mag [AB system; not including Galactic extinction of $E(B - V) = 0.069$; Schlegel et al. 1998] By comparing the position of the afterglow (as measured in the residual images) with the center of the host galaxy in the template images, we estimate an offset of $0\farcs12 \pm 0\farcs04$ (Fig. 2).

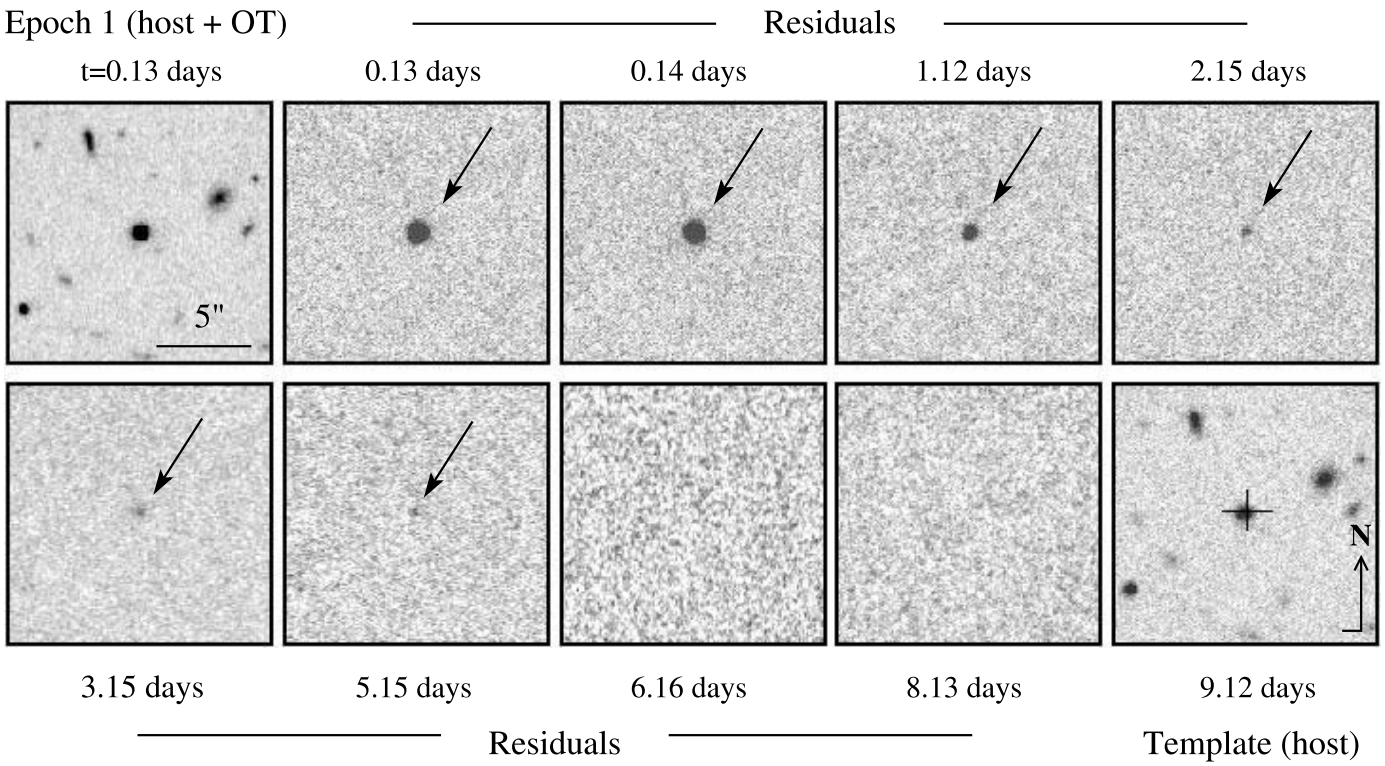

FIG. 2.—Residual images of the optical afterglow (r' band) of GRB 051221a produced through image subtraction techniques. The host galaxy emission dominates the optical light after $t \approx 2$ days. We assume that the afterglow emission is negligible in the final (*template*) epoch. The position of the afterglow (*cross*, *template image*) is offset by $0\farcs12 \pm 0\farcs04$ with respect to the host galaxy center.

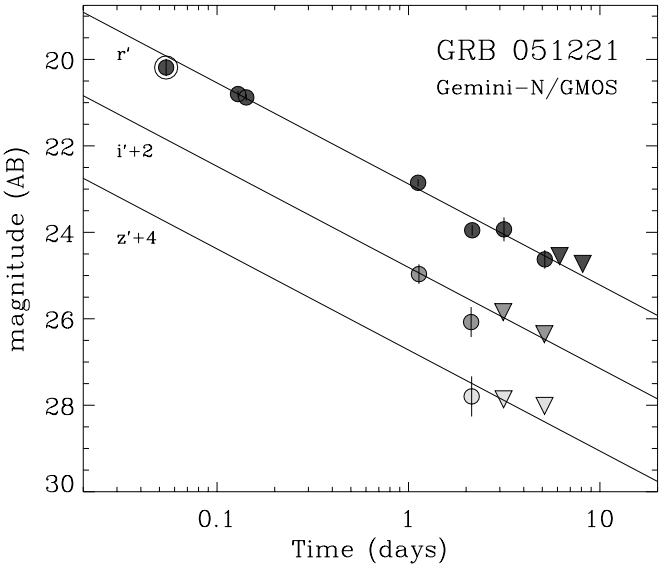

FIG. 3.—Optical ($r'i'z'$) light curves of the afterglow of GRB 051221a. We have converted the early R-band detection by Wren et al. (2005) at $t = 0.0542$ days to the r' band (*encircled dot*) using the standard zero points. The data have been corrected for Galactic extinction of $E(B - V) = 0.069$ mag (Schlegel et al.1998). The temporal evolution follows a decay index of $\alpha_{\rm opt} = -0.92 \pm 0.04$.

2.2. *Spectroscopic Observations*

Following the identification of the afterglow in our Gemini images, we used GMOS to obtain two 1200 s spectra using the R400+G5305 grating with a central wavelength of 6050 Å and a 1″ slit. The data were obtained on December 22.22 UT, about 27.5 hr after the burst. The effective wavelength coverage of our spectrum is about 5000−8170 Å with a resolution of 1.356 Å pixel^{-1} (2 × 2 binning), and a resolution element of about 3 pixels. A second observation consisting of two 1800 s spectra with the same setting was obtained on December 31.24 UT ($t \approx 10.2$ days). All observations were reduced using the standard `gmos` reduction tasks in IRAF before subtracting the sky, and combining and extracting the spectra using custom packages as described in Kelson (2003). The rms wavelength scatter is about 0.6 Å.

Flux calibration was performed using an archival observation of the spectrophotometric standard star BD +28 4211 obtained on 2005 November 17 UT. The observation was taken with the same instrumental setup as our observation of GRB 051221a, with the exception of a slight shift in the central wavelength of −50 Å. This shift was taken into account in applying the wavelength calibration, and the associated error is likely smaller than that due to slit losses. Based on our afterglow photometry (§ 2.1) and a comparison of the two spectra, we estimate that the afterglow accounts for about 40% of the total flux in the first spectrum.

As shown in Figure 4 and Table 2, we detect several emission lines in the spectrum from Hβ, [O II] λ3727, and [O III] $\lambda\lambda$4959,5006 at a redshift of $z = 0.5464 \pm 0.0001$. We detect,

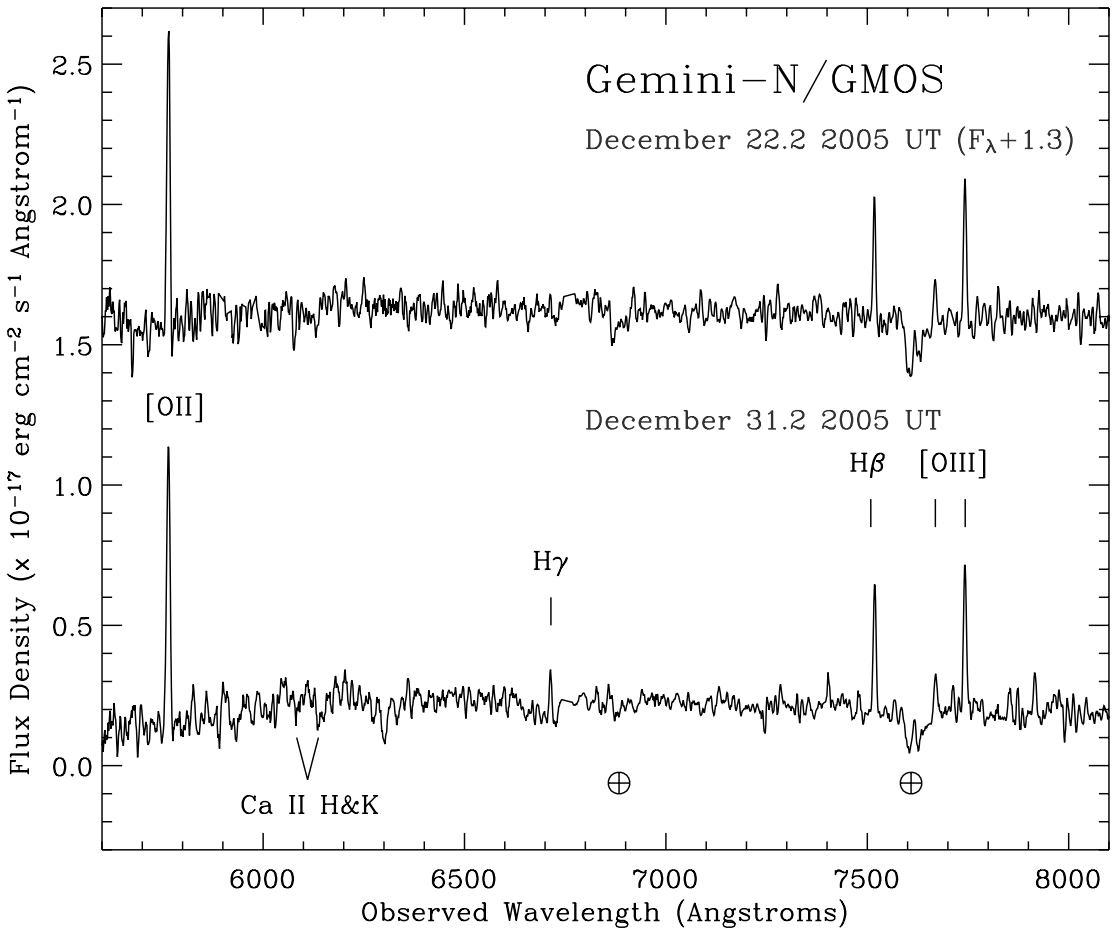

FIG. 4.—Spectrum of the host galaxy of GRB 051221a taken with Gemini-N GMOS on 2005 December 22.2 and 31.2 ($t \approx 1.1$ and 10.2 days). We detect several bright emission lines which indicate a redshift of $z = 0.5464 \pm 0.0001$ (Table 2). Absorption features attributed to Ca II H and K are also weakly detected. These features indicate that the host is an active star-forming galaxy with a significant population of older stars.

TABLE 2
SPECTROSCOPIC LINES FOR GRB 051221a

Line	λ_{rest} (Å)	λ_{obs}[a] (Å)	Redshift	Flux[b] ($\times 10^{-17}$ ergs cm^{-2} s^{-1})
[O II]	3728.48	5765.68	0.5464	10.3
Hγ	4341.69	6714.53	0.5465	1.1
Hβ	4862.69	7519.62	0.5464	3.9
[O III]	4960.24	7671.23	0.5465	1.4
[O III]	5008.24	7743.78	0.5462	4.5
Ca II K	3934.77	6082.33	0.5458	0.15[c]
Ca II H	3969.59	6136.58	0.5459	0.14[c]

[a] Observed wavelengths have been corrected to vacuum.
[b] Flux values have not been corrected for Galactic extinction.
[c] Fluxes are measured at the line bottom following the prescription of Rose 1985.

in addition, weak absorption from Ca II H and K at a redshift $z = 0.5458$. Adopting the standard cosmological parameters ($H_0 = 71$ km s^{-1} Mpc^{-1}, $\Omega_M = 0.27$, $\Omega_\Lambda = 0.73$) and a redshift of $z = 0.5464$ for the burst, the isotropic gamma-ray energy release is $E_{\gamma,\rm iso} = 4\pi F_\gamma d_L^2 (1+z)^{-1} \approx 2.4^{+0.1}_{-1.3} \times 10^{51}$ ergs (20 keV–2 MeV) where d_L is the luminosity distance. Compared with other short-hard bursts (Fox et al. 2005), the prompt energy release of GRB 051221a is a factor of $\sim$6–35 times higher.

2.3. *X-Ray Observations*

The X-ray afterglow of GRB 051221a was monitored with XRT from $t \approx 92$ s to about 11 days after the burst. We retrieved the XRT data from the HEASARC archive[12] and performed the reduction with the `xrtpipeline` script packaged within the HEAsoft software. We used the default grade selections and screening parameters to produce light curves for the 0.3–10 keV energy range. Data were rebinned using `lcurve` to produce the final afterglow light curve (Fig. 5 and Table 3). During the first $\sim$17 hr, the afterglow spectrum is well fit by a power law with $\beta_X \approx -1.0 \pm 0.2$ ($F_{\nu,X} \propto \nu^{\beta_X}$), absorbed by a neutral hydrogen column density $N_H \approx 1.6 \pm 0.6 \times 10^{21}$ cm^{-2}. This value is somewhat larger than that inferred from the Galactic extinction, assuming the standard conversion of Predehl & Schmitt (1995). These parameters are consistent with the analysis by Burrows et al. (2006).

We use the spectral parameters derived above to calibrate the light curve; we find a conversion rate of 1 count s^{-1} = 5.27×10^{-11} ergs cm^{-2} s^{-2} (0.3–10 keV). We find that the afterglow flux at $t = 10$ hr is $F_X \approx 7.5 \times 10^{-13}$ ergs cm^{-2} s^{-1}, which translates to a luminosity of $L_{X,10} \approx 5.6 \times 10^{44}$ ergs s^{-1}. This value is 1–2 orders of magnitude higher than for previous short bursts (Fox et al. 2005) and is in the range typical of the long-duration events (Berger et al. 2003a). Our analysis of the full XRT data set between $t \approx 92$ s and 11 days shows that the evolution of the X-ray afterglow can be characterized by three phases: an initial fading as $F_X \propto t^{\alpha_X}$ with $\alpha \approx -1.07 \pm 0.03$, a brief plateau phase between $t \sim 0.05$ and 0.13 days, and a subsequent decay as $\alpha_X \approx -1.06 \pm 0.04$. We emphasize that the decay indices before and after the plateau phase are identical, suggesting a simple evolution interrupted by an injection of energy (§ 3.3).

[12] See http://heasarc.gsfc.nasa.gov/W3Browse/.

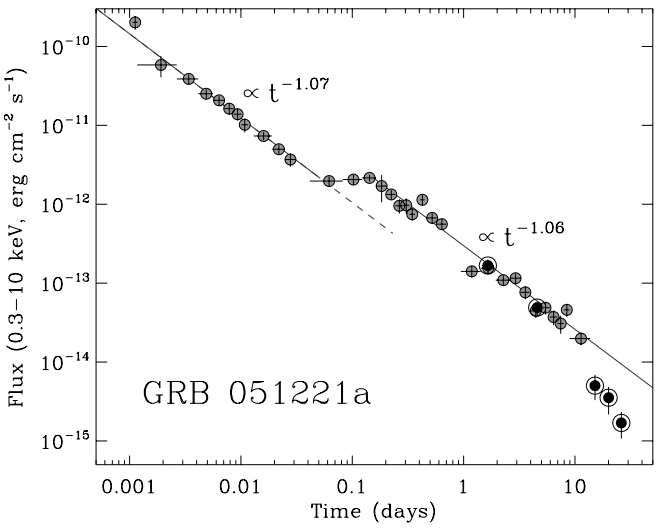

FIG. 5.—Light curve of the X-ray afterglow of GRB 051221a as observed with *Swift* XRT (*gray circles*) and *Chandra* ACIS-S (*encircled black dots*; Burrows et al. 2006) from $t \approx 92$ s to 26 days after the burst. The light curve is characterized by four phases: an initial decay with index $\alpha_X = -1.07 \pm 0.03$, a brief plateau phase, a subsequent decay with $\alpha_X = -1.06 \pm 0.04$, and steepening at $t \approx 5$ days. An extrapolation of the early decay to $t \sim 1$ day indicates an increase in flux by a factor of $\sim$3.3 corresponding to an energy injection of a factor of $\sim$3.4. We interpret the late-time steepening as a jet break and derive a collimation angle of $\theta_j \approx 7^\circ$.

TABLE 3
Swift XRT OBSERVATIONS OF GRB 051221a

Δt (days[a])	Sample Time (days)	F_X (0.3–10 keV) (ergs cm^{-2} s^{-1})	σ (ergs cm^{-2} s^{-1})
1.12×10^{-3}	1.16×10^{-4}	2.02×10^{-10}	3.82×10^{-11}
1.91×10^{-3}	1.48×10^{-3}	5.83×10^{-11}	1.76×10^{-11}
3.40×10^{-3}	1.48×10^{-3}	3.88×10^{-11}	5.54×10^{-12}
4.88×10^{-3}	1.48×10^{-3}	2.51×10^{-11}	3.33×10^{-12}
6.37×10^{-3}	1.48×10^{-3}	2.08×10^{-11}	2.91×10^{-12}
7.85×10^{-3}	1.48×10^{-3}	1.63×10^{-11}	2.57×10^{-12}
9.34×10^{-3}	1.48×10^{-3}	1.38×10^{-11}	2.37×10^{-12}
1.08×10^{-2}	1.48×10^{-3}	1.02×10^{-11}	2.03×10^{-12}
1.60×10^{-2}	5.93×10^{-3}	7.33×10^{-12}	8.63×10^{-13}
2.19×10^{-2}	5.93×10^{-3}	4.98×10^{-12}	7.19×10^{-13}
2.78×10^{-2}	5.93×10^{-3}	3.68×10^{-12}	6.96×10^{-13}
6.19×10^{-2}	4.05×10^{-2}	1.97×10^{-12}	2.78×10^{-13}
0.102	4.05×10^{-2}	2.06×10^{-12}	2.97×10^{-13}
0.143	4.05×10^{-2}	2.16×10^{-12}	2.21×10^{-13}
0.183	4.05×10^{-2}	1.70×10^{-12}	6.43×10^{-13}
0.223	4.05×10^{-2}	1.33×10^{-12}	1.75×10^{-13}
0.264	4.05×10^{-2}	9.55×10^{-13}	1.95×10^{-13}
0.305	4.05×10^{-2}	9.71×10^{-13}	2.17×10^{-13}
0.345	4.05×10^{-2}	7.46×10^{-13}	1.28×10^{-13}
0.427	4.05×10^{-2}	1.14×10^{-12}	1.70×10^{-13}
0.522	0.116	6.71×10^{-13}	9.69×10^{-14}
0.638	0.116	5.59×10^{-13}	8.63×10^{-14}
1.18	0.480	1.41×10^{-13}	2.29×10^{-14}
1.66	0.480	1.55×10^{-13}	2.45×10^{-14}
2.27	0.656	1.09×10^{-13}	1.65×10^{-14}
2.93	0.656	1.15×10^{-13}	1.67×10^{-14}
3.58	0.656	7.64×10^{-14}	1.40×10^{-14}
4.45	0.990	4.45×10^{-14}	8.57×10^{-15}
5.44	0.990	4.88×10^{-14}	8.92×10^{-15}
6.42	0.990	3.72×10^{-14}	7.93×10^{-15}
7.44	0.957	3.08×10^{-14}	7.94×10^{-15}
8.45	0.953	4.58×10^{-14}	8.82×10^{-15}
11.33[b]	4.72	1.99×10^{-14}	3.48×10^{-15}

[a] Δt values give at midexposure time.
[b] Co-addition of multiple observations.

TABLE 4
Radio Observations of GRB 051221a

Date Obs (UT)	Δt (days)	$F_{\nu,8.46\,\mathrm{GHz}}$ (μJy)	$\sigma_{8.46\,\mathrm{GHz}}$[a] ($\mu$Jy)
2005 Dec 21.99	0.91	155	$\pm$ 30
2005 Dec 23.02	1.94	...	$\pm$ 24
2005 Dec 24.83	3.75	...	$\pm$ 32
2005 Dec 27.96	6.88	...	$\pm$ 28
2006 Jan 14.01	23.93	...	$\pm$ 16

[a] All errors are given as 1 σ (rms).

2.4. *Radio Observations*

We initiated radio observations of GRB 051221a with the Very Large Array[13] (VLA) on 2005 December 21.99 UT. The data were obtained at 8.46 GHz covering the range 0.91–23.93 days (see Table 4). All observations were taken in standard continuum observing mode with a bandwidth of 2×50 MHz. We used 3C 48 (J0137+331) for flux calibration, while phase referencing was performed against calibrator J2152+175. The data were reduced using standard packages within the Astronomical Image Processing System (AIPS).

We detect a radio source coincident with the optical position with a flux $F_\nu = 155 \pm 30$ μJy in the first observation. The source subsequently faded below our detection threshold with a decay rate of $\alpha_{\rm rad} \lesssim -1.0$.

3. AFTERGLOW PROPERTIES

Using the detailed multifrequency observations of the GRB 051221a afterglow we proceed to constrain the physical properties of the ejecta and the circumburst density. We assume that, like the afterglows of long GRBs, the afterglows of short bursts are produced through the dynamical interaction of the ejecta with the surrounding medium (the forward shock [FS]) with an additional component from shock heating of the ejecta (the reverse shock [RS]). This assumption is consistent with the existing afterglow data for short bursts (Berger et al. 2005; Bloom et al. 2006; Fox et al. 2005; Panaitescu 2006). In this scenario, the total energy density is partitioned between relativistic electrons, ϵ_e, and magnetic fields, ϵ_B, while the thermal energy of the shocked protons accounts for the fraction remaining (see Piran 1999 for a review). The shocked electrons are accelerated into a power-law distribution, $N(\gamma) \propto \gamma^{-p}$, above a minimum Lorentz factor, γ_m. The emission resulting from the forward and reverse shock components is described by a synchrotron spectrum characterized by three break frequencies—the self-absorption frequency, ν_a; the characteristic frequency, ν_m; and the cooling frequency, ν_c—and a flux normalization, F_{ν_m} (Sari et al. 1998). In modeling the afterglow spectral and temporal evolution, we adopt the formalism of Granot & Sari (2002) for a relativistic forward shock expanding into a constant density circumburst medium and the scalings of Sari & Piran (1999) for a mildly relativistic reverse shock.

3.1. *Preliminary Constraints*

We proceed to fit the forward shock model to the afterglow data using only observations at $t \gtrsim 0.1$ day in the X-rays and $t \gtrsim 1$ day in the radio when the afterglow evolution follows a simple power law. As shown in § 3.3, the data prior to $t \sim 0.1$ days in the X-ray band are influenced by energy injection while the radio detection at $t \approx 0.91$ days, and the subsequent decline are inconsistent with a simple forward shock model and are instead explained in the context of reverse shock emission.

To constrain the spectrum of the forward shock, we first investigate the evolution in the optical and X-ray bands. From the X-ray data we measure $\alpha_{\rm X} = -1.06 \pm 0.04$ and $\beta_{\rm X} = -1.0 \pm 0.2$, leading to $\alpha - 3\beta/2 = 0.44 \pm 0.23$. A comparison to the standard closure relations (see Sari et al. 1998), $\alpha - 3\beta/2 = 0$ ($\nu_m < \nu < \nu_c$) and $\alpha - 3\beta/2 = 1/2$ ($\nu > \nu_c$), indicates that $\nu_{\rm X} > \nu_c$. These conclusions are supported by the optical to X-ray spectral slope, $\beta_{\rm ox} = -0.64 \pm 0.05$ (after correcting the optical data for Galactic extinction), which is flatter than $\beta_{\rm X}$ as expected if $\nu_{\rm opt} < \nu_c < \nu_{\rm X}$. In addition, the optical decay rate, $\alpha_{\rm opt} = -0.92 \pm 0.04$, is somewhat shallower than $\alpha_{\rm X}$, as expected if ν_c is between the two bands. We note that this also supports our assumption of a constant-density medium, since in a wind environment the expected value of $\alpha_{\rm opt}$ is about -1.3, significantly steeper than the observed value. Using all the available optical and X-ray observations, we find that $p = 2.15 \pm 0.10$ and $\nu_c = (2 \pm 1) \times 10^{17}$ Hz at $t = 1$ day. Here and throughout this section we have accounted for the smooth shape of the spectral breaks, and we note that in this context the values of F_{ν_m} quoted below are the asymptotic extrapolations.

Next we compare the optical and radio afterglow data to constrain ν_m and the peak spectral flux, F_{ν_m}. The single power-law optical decay constrains ν_m to be lower than the optical band before the first observation at $t = 0.0542$ days, and F_{ν_m} to be above the flux of the first observation. Scaling these constraints to $t = 1$ day ($\nu_m \propto t^{-1.5}$ and $F_{\nu_m} \propto t^0$) we find $\nu_m \lesssim 1.5 \times 10^{12}$ Hz and $F_{\nu_m} \gtrsim 74$ μJy. Furthermore, we note that the two constraints are linked through the relation $F_{\nu_m} \propto \nu_m^{-(p-1)/2}$ such that lower values of ν_m imply increasingly higher values of F_{ν_m}.

Given the link between ν_m and F_{ν_m}, we obtain a lower bound on ν_m (and hence an upper bound on F_{ν_m}) from the limits on the radio flux at $t \gtrsim 1$ day. In particular, the 3 σ limits of $\lesssim$80 μJy at $t \sim$ 2–7 days indicate that $\nu_m \gtrsim 4.0 \times 10^{11}$ Hz and $F_{\nu_m} \lesssim 160$ μJy at $t = 1$ day; otherwise, the forward shock flux would be brighter than the observed radio limits. Combined with the optically derived limits, we therefore find the allowed ranges of $4.0 \times 10^{11} \lesssim \nu_m \lesssim 1.5 \times 10^{12}$ Hz and $74 \lesssim F_{\nu_m} \lesssim 160$ μJy at $t = 1$ day.

3.2. *Forward Shock Broadband Model*

Adopting these preliminary constraints on ν_m and F_{ν_m} and using the derived value of ν_c, we apply a broadband afterglow model fit to the multifrequency data in order to determine the physical parameters of the burst. The four spectral parameters (F_{ν_m}, ν_a, ν_m, and ν_c) are fully determined by four physical quantities: the kinetic energy of the ejecta, $E_{K,\rm iso}$; the energy partition fractions, ϵ_e and ϵ_B; and the circumburst density, n. Therefore, by constraining the four spectral parameters through broadband observations, we are able to determine a unique solution for the four physical parameters. Although ν_a is not directly constrained by the observations, we are able to define a range of reasonable solutions by requiring that ϵ_e, $\epsilon_B \leq 1/3$, which accounts for an equal (or larger) contribution from shocked protons ($\epsilon_p \geq 1/3$). This requirement excludes unphysical solutions in which the sum of the contributions from shocked electrons, protons, and magnetic fields exceed the total energy density. With this constraint on the energy partition fractions, and the

[13] The Very Large Array and Very Long Baseline Array are operated by the National Radio Astronomy Observatory, a facility of the National Science Foundation operated under cooperative agreement by Associated Universities, Inc.

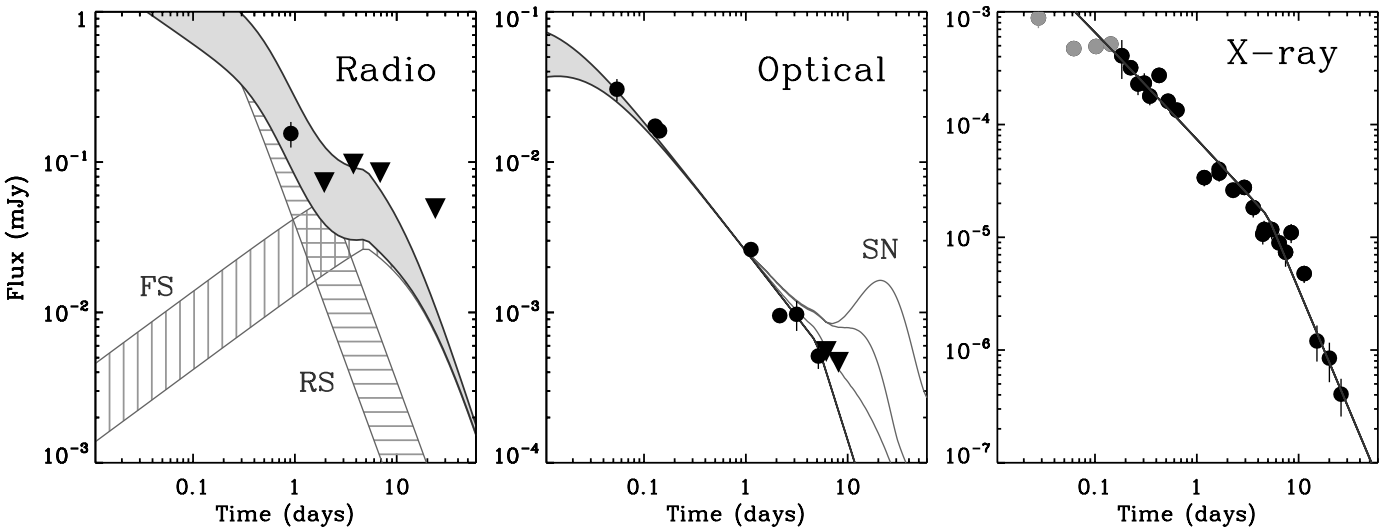

FIG. 6.—Broadband afterglow model fits for the radio (8.5 GHz), optical (r' band) and X-ray data of GRB 051221a based on the inferred constraints discussed in § 3.2. Detections are shown as filled circles and upper limits are plotted as inverted triangles. The r'-band data have been corrected for Galactic extinction. Black lines designate the forward shock contribution while the shaded region in the radio includes the allowed range of $\nu_m^{\rm FS}$ and $F_{\nu_m}^{\rm FS}$ (see also optical band) and the reverse shock emission associated with the energy injection episode in the X-rays at $t \sim 0.1$ days. Overplotted in the optical panel are the predicted light curves including the contribution from Type Ibc SNe 1998bw, 1994I, and 2002ap (*thin gray lines, top to bottom, respectively*). The late-time optical limits clearly rule out the presence of a bright SN 1998bw–like event and constrain the peak optical magnitude to $M_V \gtrsim -17.2$ mag (rest frame), consistent with a faint event similar to SN 2002ap. A jet break is observed at $t \approx 5$ days, causing an achromatic steepening of the afterglow light curves.

observed estimates for F_{ν_m}, ν_m, and ν_c from § 3.1, we find the following ranges for the physical parameters:

$$1.1 \times 10^{51} \lesssim E_{K,\rm iso} \lesssim 4.4 \times 10^{51} \text{ ergs} \quad (1a)$$

$$2.8 \times 10^{-4} \lesssim n \lesssim 1.5 \times 10^{-1} \text{ cm}^{-3} \quad (1b)$$

$$9.5 \times 10^{-2} \lesssim \epsilon_e \leq 1/3 \quad (1c)$$

$$7.8 \times 10^{-3} \lesssim \epsilon_B \leq 1/3. \quad (1d)$$

3.3. *Energy Injection and Reverse Shock Model*

We now turn to the X-ray plateau phase observed between $t \approx 1$ and 3 hr after the burst. The flattening of the light curve suggests that GRB 051221a experienced an episode of energy injection on this timescale. As shown in Figure 5, an extrapolation of the early decay lies a factor of about 3.3 below the observed flux after the plateau phase. Given that ν_c is located below the X-ray band on this timescale, we have $F_{\nu,\rm X} \propto E^{(p+2)/4}$. Thus, for $p = 2.15$ the flux increase corresponds to an energy injection of a factor of ~3.4. We note that given the flat X-ray evolution during the energy injection phase, the ejecta refreshing the shock follows the relation $E(>\gamma) \propto \gamma^{-4.5}$ (Sari & Mészáros 2000).

One implication of this energy injection episode is emission from the associated reverse shock (Sari & Mészáros 2000). The broadband spectrum of the reverse shock differs from that of the forward shock spectrum primarily due to its lower characteristic frequency, $\nu_m^{\rm RS} \approx \nu_m^{\rm FS}/\gamma^2$, and its higher spectral peak flux, $F_{\nu_m}^{\rm RS} \approx \gamma F_{\nu_m}^{\rm FS}$. Here, the bulk Lorentz factor of the ejecta is given by $\gamma \approx 8.3(E_{K,\rm iso}/10^{51}\ \text{erg})^{1/8}(n/10^{-3}\ \text{cm}^{-3})^{-1/8}(t/1\ \text{day})^{-3/8}$.

Adopting the constraints for $\nu_m^{\rm FS}$ and $F_{\nu_m}^{\rm FS}$ (along with the associated constraints on $E_{K,\rm iso}$ and n) from § 3, we find that at the time of the energy injection episode ($t \sim 0.1$ days) $18 \lesssim \gamma \lesssim 26$ and thus $2.0 \times 10^{10} \lesssim \nu_m^{\rm RS} \lesssim 1.5 \times 10^{11}$ Hz and $1.3 \lesssim F_{\nu_m}^{\rm RS} \lesssim 4.1$ mJy. Using the temporal scalings of Sari & Piran (1999), $\nu_m^{\rm RS} \propto t^{-73/48}$ and $F_{\nu_m}^{\rm RS} \propto t^{-47/48}$, we find that $\nu_m^{\rm RS}$ is just below 8.46 GHz during our first radio observation. We therefore estimate $47 \lesssim F_{\nu,8.46\,\rm GHz}^{\rm RS} \lesssim 295$ μJy at $t \approx 0.91$ days, which is fully consistent with our measured flux of $F_{\nu,8.46} = 155 \pm 30$.

The radio RS component is then predicted to decay rapidly as $F_\nu \propto t^{-1.85}$, implying an estimated flux at $t = 1.94$ days (our second radio epoch) of $12 \lesssim F_{\nu,8.46\,\rm GHz}^{\rm RS} \lesssim 73$ μJy, again consistent with our measured limit of $F_{\nu,8.46} \lesssim 72$ μJy. We therefore conclude that the X-ray plateau phase at $t \sim 0.1$ day and the early radio decay are the result of an energy injection episode. We note that this interpretation predicts a 4.86 GHz flux density at $t \approx 0.6$ days that is a factor of ~2 above the measured limit of van der Horst (2005). However, this can be explained as the result of synchrotron self-absorption, since for the reverse shock, $\nu_a^{\rm RS} \approx \gamma^{8/5}\nu_a^{\rm FS}$ can be as high as 5 GHz at $t = 0.6$ days given our allowed range of $\nu_a^{\rm FS}$.

3.4. *A Combined FS+RS Model*

In Figure 6 we show the combined FS+RS light curves and we find that given the contribution of the reverse shock emission in the radio band we can limit the range of allowed physical parameters beyond the constraints provided in equations (1a) to (1d). Using the observed upper limits, we therefore favor the fainter end of the allowed FS model corresponding to the parameters $\nu_m^{\rm FS} \approx 1.5 \times 10^{12}$ Hz and $F_{\nu_m}^{\rm FS} \approx 74$ μJy at $t = 1$ day. This provides constraints on the physical parameters of $E_{K,\rm iso} \approx (1.1\text{–}1.6) \times 10^{51}$ ergs, $n \approx (0.5\text{–}2.4) \times 10^{-3}$ cm^{-3}, $\epsilon_e \approx (0.24\text{–}0.33)$, and $\epsilon_B \approx (0.12\text{–}0.33)$.

These improved constraints lead to the following implications. First, the efficiency in converting the energy in the ejecta into gamma-rays is $\eta_\gamma \approx 0.6\text{–}0.7$, indicating a roughly equal partition in prompt and afterglow energy, similar to what is found for long GRBs (Panaitescu & Kumar 2002). Second, we find that the shock energy is in rough equipartition between relativistic electrons and magnetic fields. This is consistent with the values inferred for long-duration GRBs (Yost et al. 2003; Panaitescu & Kumar 2002).

TABLE 5
PHYSICAL PARAMETERS FOR GRB 051221a

Parameter	Value
$E_{\gamma,\rm iso}$	$2.4^{+0.1}_{-1.3} \times 10^{51}$ ergs
$E_{K,\rm iso}$	$(1.1–1.6) \times 10^{51}$ ergs
n	$(0.5–2.4) \times 10^{-3}$ cm^{-3}
ϵ_e[a]	(0.24–1/3)
ϵ_B[a]	(0.12–1/3)
θ_j	(5.7°–7.3°)
f_b	(0.005–0.008)
E_γ	$(1.2–1.9) \times 10^{49}$ ergs
E_K	$(7.8–8.9) \times 10^{48}$ ergs

[a] Values are constrained to be $<1/3$.

3.5. *A Jet Break*

Using late-time *Chandra* ACIS-S observations extending to 26 days, Burrows et al. (2006) find strong evidence for a steepening in the X-ray afterglow light-curve, which they attribute to a jet break. By supplementing our optical, XRT, and radio data with the late-time *Chandra* observations, we are able to constrain the opening angle of the jet and thus derive the beaming-corrected energy of the burst. As shown in Figure 5, the first two *Chandra* epochs at $t \approx 1.7$ and 4.6 days are consistent with the *Swift* XRT measurements and the inferred decay of $\alpha_{\rm X} \approx -1.06$. However, the last three *Chandra* points at $t \gtrsim 15$ days show a steeper decay, $\alpha_{\rm X} = -2.0 \pm 0.4$, which is consistent with the expected decay rate in the case of a jet break, $\alpha_{\rm X} = -p \approx -2.15$ (Sari et al. 1999). By fitting the radio, optical and X-ray data together, we modify our spherical FS+RS model to include a jet break and find a best fit for a smooth break at $t_j \approx 5$ days, consistent with the findings of Burrows et al. (2006). As shown in Figure 6, this model provides an excellent fit to the entire broadband data set.

Together with the physical parameters derived in § 3.4, the observed jet break constrains the collimation of the ejecta to $\theta_j \approx 6.6(E_K/10^{51}\ {\rm ergs})^{-1/8}(n/10^{-3}\ {\rm cm}^{-3})^{1/8} \approx (5\overset{\circ}{.}7–7\overset{\circ}{.}3)$. This indicates that the true energy release is $E_\gamma \approx (1.2–1.9) \times 10^{49}$ ergs and $E_K \approx (7.8–8.9) \times 10^{48}$ ergs, or a total relativistic energy yield of $(E_\gamma + E_K) \approx (2–3) \times 10^{49}$ ergs. We summarize the final parameters for GRB 051221a in Table 5 and note that they are generally consistent with those reported by Burrows et al. (2006). Finally, we find that the ejecta will become nonrelativistic on a timescale $t_{\rm NR} \approx 2.0(E_K/10^{51})^{1/3}(n/10^{-3}\ {\rm cm}^{-3})^{-1/3} \approx (0.3–0.5)$ yr.

3.6. *Limits on an Associated Supernova*

The optical afterglow measurements at late time can also be used to constrain the contribution from an associated supernova. To assess this contribution we adopt the optical data for the local Type Ibc SNe 1994I (Richmond et al. 1996), 1998bw (Galama et al. 1998; McKenzie & Schaefer 1999), and 2002ap (Foley et al. 2003) as templates. These three SNe were selected based on their well-sampled optical light curves and peak luminosities, which represent the overall spread in the observed properties of Type Ibc supernovae. To produce synthesized light curves for each of these template SNe, we compiled optical *UBVRI* observations from the literature and smoothed the extinction-corrected (foreground plus host galaxy) light curves. We then produced *k*-corrected light curves by redshifting the interpolated photometric spectrum and stretching the arrival time of the photons by a factor of $(1 + z)$. A full discussion of the template data sets and the method by which we produce the synthetic SN light curves appears in Soderberg et al. (2005).

Shown in Figure 6 are the synthesized r'-band light curves for these three supernovae at the redshift of GRB 051221a (roughly equivalent to the rest-frame *B*-band SN emission). These light curves represent the summed contribution from the afterglow and SN models. Clearly, our late-time optical measurements rule out the presence of the brighter two SNe (1998bw and 1994I), while our limits are consistent with a faint SN 2002ap–like event with a peak optical magnitude of $M_V \gtrsim -17.2$ (rest frame) corresponding to a limit on the mass of synthesized nickel of $\lesssim 0.07\ M_\odot$ (Mazzali et al. 2002). We note, however, that the bright afterglow flux at $t \lesssim 1$ day can easily hide the emission from a mildly relativistic "macronova" for a wide range of ejecta velocities and energies (Kulkarni 2005), and we therefore cannot assess the contribution from such a component. Finally, we note that no SN absorption features were observed in the spectrum taken at $t \approx 10.2$ days at which time a typical Type Ibc SN would reach maximum light.

4. HOST GALAXY PROPERTIES

We now turn to the properties of the GRB host galaxy. We measure the brightness of the host galaxy using our final epoch template images (Table 1) and find $r' = 21.99 \pm 0.09$ mag, $i' = 21.99 \pm 0.17$ mag, and $z' = 21.97 \pm 0.40$ mag; all magnitudes are in the AB system and have been corrected for Galactic extinction, $E(B - V) = 0.069$ mag, and the uncertainties are dominated by the photometric calibration. The spectral slope based on these magnitudes is nearly flat in F_ν. At the redshift of the host galaxy, the rest-frame *V* band is traced by the combination of the i' and z' bands, leading to an absolute magnitude $M_V \approx -20.0 \pm 0.3$ mag, while the rest-frame *B* band is traced by the r' band indicating $M_B \approx -19.9 \pm 0.1$ mag, or a luminosity $L_B \approx 0.3L_*$. This luminosity is similar to those of the host galaxies of many long GRBs, as well as the host galaxy of the short GRB 050709 with $L \approx 0.1L_*$ (Fox et al. 2005).

We further use `galfit` (Peng et al. 2002) to examine the surface brightness profile of the host galaxy. We use nearby stars to construct a point-spread function image for the deconvolution process and find that the best-fit scale length is about 420 ± 50 mas, or about 2.6 ± 0.3 kpc, and the Sersic index is about 0.6, close to the value of 1 for an exponential disk, but significantly different from a value of 4, appropriate for elliptical galaxies. The morphological parameters are again similar to those found for the hosts of long-duration GRBs (Wainwright et al. 2005).

At $z = 0.5464$, the measured offset of the afterglow (§ 2.1) relative to the center of the host galaxy corresponds to 760 ± 30 pc. Normalized by the scale length of the galaxy this corresponds to $r/r_e = 0.29 \pm 0.04$. This offset is somewhat smaller than those measured for previous short GRBs (Fox et al. 2005) and continues the trend of smaller offsets compared to predictions from population synthesis models. For example, Fryer et al. (1999a) predict that $<1\%$ of short GRBs will have offsets less than 2 kpc. We note, however, that smaller offsets are possible for merger events within star-forming galaxies, which may have small initial binary separations (Belczynski et al. 2002).

As shown in Figure 4, the host exhibits both emission lines and Ca II H and K absorption features. Using our late-time spectrum in which the afterglow contribution is negligible, we estimate the star formation rate in the host galaxy from the observed fluxes of the various emission lines. From the flux of the [O II] λ3727 line, $F_{[\rm O\ II]} = 1.3 \times 10^{-16}$ ergs cm^{-2} s^{-1} (Table 2), and the conversion of Kennicutt (1998), ${\rm SFR} = (1.4 \pm 0.4) \times 10^{-41} L_{[\rm O\ II]}$, we find a star formation rate of about $2.0 \pm 0.5\ M_\odot\ {\rm yr}^{-1}$. From the H$\beta$ line flux, $F_{\rm H\beta} \approx 4.5 \times 10^{-17}$ ergs cm^{-2} s^{-1}, and assuming the case B recombination ratio of $F_{\rm H\alpha}/F_{\rm H\beta} = 2.85$, we infer a star

formation rate of about 1.2 $M_\odot$ yr^{-1}. Thus, we conclude that the star formation rate (not corrected for host extinction) is about $1.6 \pm 0.4\ M_\odot\ \mathrm{yr}^{-1}$. We note that the measured ratio of Hγ/H$\beta \sim 0.3$, compared to the theoretical value of about 0.47 (Osterbrock 1989), may point to an extinction correction of the star formation rate of about a factor of 2. The inferred star formation rate is not atypical for the hosts of long GRBs, but is about a factor of 6 larger than in the star-forming host of the short GRB 050709 (Fox et al. 2005). Moreover, it exceeds by at least a factor of 20–30 the limits on the star formation rates in the elliptical hosts of GRBs 050509b and 050724 (Berger et al. 2005; Bloom et al. 2006; Prochaska et al. 2006).

The combination of the inferred star formation rate and host luminosity provides a measure of the specific star formation rate. We find a value of $4\ M_\odot\ \mathrm{yr}^{-1}\ L_*/L$, which is about a factor of 2.5 times lower than the mean specific star formation rate for the hosts of long-duration GRBs (Christensen et al. 2004). This indicates that the star formation activity in the host of GRB 051221a is less intense than in a typical long GRB host galaxy.

The detection of Ca II H and K absorption lines indicates that while the host is undergoing current star formation, at least some fraction of the light arises from an old population of stars. The relative strengths of the two Ca II lines provide an indication of the age of the stellar population. Following the approach of Rose (1985), we find that the ratio of Ca II H and Hϵ to Ca II K is about unity. This value is typical for stars with spectral type later than F; for earlier type stars Ca II reversal takes place. An accurate decomposition of the fractions of old and new stars is difficult to achieve given that these features are only weakly detected. Still, a contribution from a stellar population with an age of $\sim$1 Gyr is suggested.

Finally, we use the relative strengths of the oxygen and hydrogen emission lines to infer the ionization state and oxygen abundance. The relevant indicators are $R_{23} \equiv \log (F_{[\mathrm{O\ II}]} + F_{[\mathrm{O\ II}]}/F_{\mathrm{H}\beta}) \approx 0.62$ and $O_{32} \equiv \log (F_{[\mathrm{O\ II}]}/F_{[\mathrm{O\ II}]}) \approx -0.24$. Using the calibration of McGaugh (1991), we find that the for the upper branch the metallicity is $12 + \log (\mathrm{O/H}) \approx 8.7$, while for the lower branch it is about 8.2; the two branches are due to the double-valued nature of R_{23} in terms of metallicity. Thus, the host metallicity is 0.3–1 $Z_\odot$. This is somewhat higher than in the host galaxies of long GRBs, some of which have metallicities that are $\sim$1/10 $Z_\odot$ (e.g., Prochaska et al. 2004). This supports the conclusion that the stellar population in the host galaxy of GRB 051221a is more evolved than that in the host galaxies of long GRBs.

To summarize, we find that the host galaxy of GRB 051221a is undergoing active star formation with a rate and intensity at the low end of the distribution for the hosts of long GRBs, but larger than all previous hosts of short GRBs. The active star formation with an [O II] equivalent width of about 36 Å, signs of an old stellar population from the Ca II H and K absorption, and a non-detected Balmer/4000 Å break indicate a classification intermediate between e(b) and e(c) in the classification scheme of Dressler et al. (1999). Along with a nearly solar metallicity, the host galaxy of GRB 051221a appears to have a relatively evolved population of stars. This continues to support the trend that the progenitors of short bursts arise from old stellar populations, but given the higher star formation rate compare to previous short burst hosts leaves open the possibility that the progenitor lifetimes span a wide range.

5. DISCUSSION AND CONCLUSIONS

We present broadband optical, radio, and X-ray data for the afterglow of the short-hard burst GRB 051221a. Due to our rapid identification of the afterglow we were able to obtain a spectrum at $t \approx 1.1$ day when the afterglow was, in principle, sufficiently bright to detect absorption features from the interstellar medium of the host galaxy leading to a direct redshift measurement. Unfortunately, at the redshift of the host galaxy, $z = 0.5464$, no strong metal UV lines are redshifted into the wave band of our spectrum. Still, rapid identification and spectroscopy of future short bursts may potentially lead to direct redshift measurements.

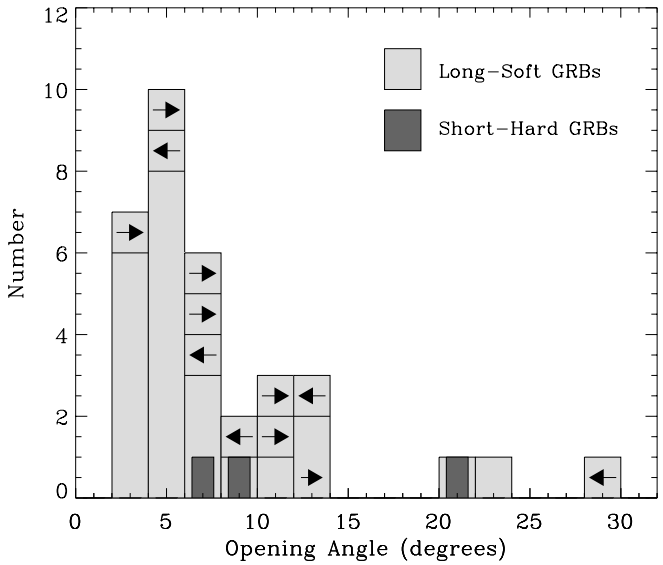

FIG. 7.—Collimation angles for long (Berger et al. 2003a; Bloom et al. 2003; Ghirlanda et al. 2004 and references therein) and short (GRB 050709: Fox et al. 2005; GRB 050724: Berger et al. 2005; GRB 051221a: this paper) GRBs are compiled from the literature. All three short bursts have opening angles larger than 5° which is the median value for long bursts.

At $z = 0.5464$, GRB 051221a currently represents the most distant short GRB for which we have a secure redshift. More importantly, we emphasize that GRB 051221a is only the third short burst for which a detailed afterglow study has been performed and the physical parameters have been constrained. The isotropic-equivalent gamma ray and kinetic energy releases are 2.4×10^{51} and 1.4×10^{51} ergs respectively. These values are a factor of 10 and 10^2 times larger than the values for the short GRBs 050724 and 050709, respectively.

Adopting the results of our standard synchrotron model and using $t_j \approx 5$, we constrain the collimation of the ejecta to $\theta_j \approx 7°$, comparable to the opening angles of GRBs 050709 and 050724 (Fox et al. 2005; Berger et al. 2005; Panaitescu 2006; but see Grupe et al. 2006). A comparison to the compilation of jet opening angles of long GRBs, shown in Figure 7, demonstrates that while overlap exists between the two distributions, the opening angles measured for the three short GRBs are about a factor of 2 larger than the median value of 5° for long GRBs. This may not be surprising given that in the case of long GRBs the passage of the jet through the stellar envelope is thought to be responsible for its collimation (Zhang et al. 2003). On the other hand, in models of compact object mergers it has been argued that the outflow may be collimated by a neutrino-driven wind (Rosswog et al. 2003) or the accretion disk itself (Aloy et al. 2005), both of which lead to relatively wide opening angles, $\gtrsim 10°$. Most likely the same holds true for scenarios such as accretion-induced collapse of a neutron star or a white dwarf (Yi & Blackman 1998; Fryer et al. 1999b).

With the inferred opening angle, the beaming-corrected energy of GRB 051221a is similar to those of previous short bursts and

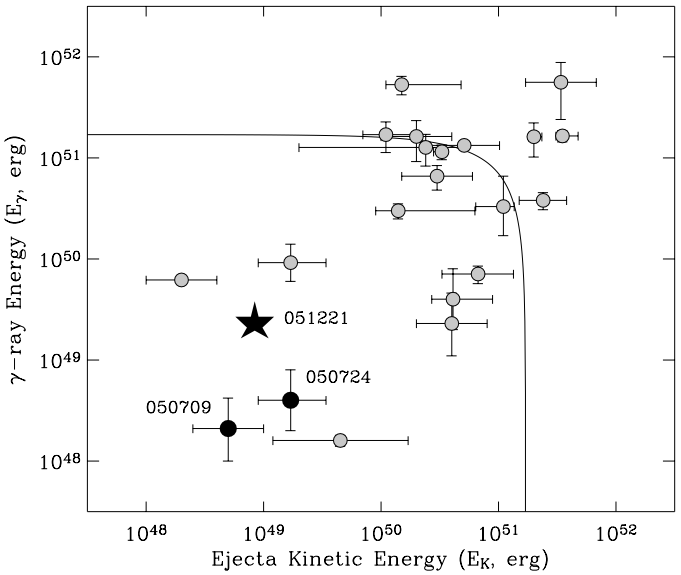

FIG. 8.—Energy release in prompt gamma-ray emission plotted against the total kinetic energy of the ejecta for long GRBs (*gray circles*; Bloom et al. 2003; Ghirlanda et al. 2004; Sazonov et al. 2004; Soderberg et al. 2006a, 2006 and references therein) and short bursts (*black circles*; GRB 050709: Fox et al. 2005; GRB 050724: Berger et al. 2005) as inferred from broadband afterglow modeling. Both axes are corrected for collimation of the ejecta. The total energy release (prompt plus afterglow) of long bursts cluster near 1.7×10^{51} ergs (*black solid arc*). GRB 051221a (*star*) has a total energy comparable to short GRBs 050724 and 050709.

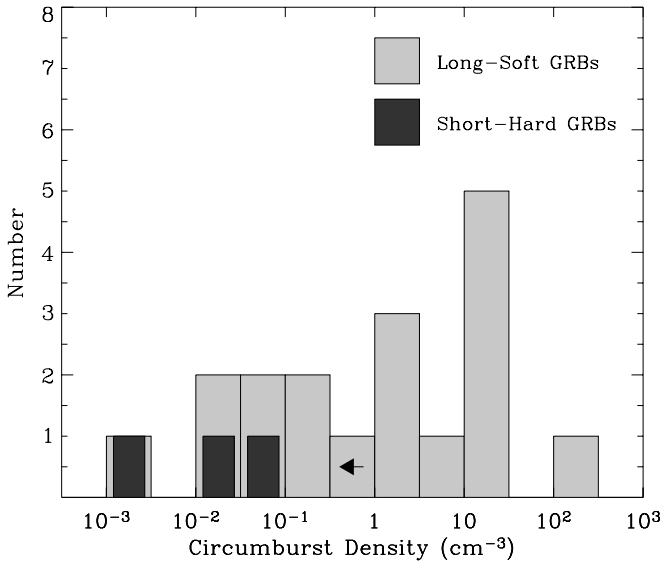

FIG. 9.—Circumburst density values for long (Soderberg et al. 2006a and references therein) and short (GRB 050709: Fox et al. 2005; GRB 050724: Berger et al. 2005; GRB 051221a: this paper) GRBs are shown as a histogram. While long bursts show a wide range of circumburst densities, the short events cluster toward lower values. This can be understood in terms of their different progenitors and environments.

comparable to the low end of the distribution for long-duration events (e.g., GRB 031203; Sazonov et al. 2004; Soderberg et al. 2004). This is shown in Figure 8, where we compile the beaming-corrected gamma ray energy release and ejecta energy values for both long- and short-duration bursts. It has been argued that the majority of the long GRBs have a total (prompt plus afterglow) true energy release within 0.5 dex of 1.7×10^{51} ergs (Berger et al. 2003b), with three events having a total energy of $\lesssim 10^{50}$ ergs (Soderberg et al. 2004, 2006). The similar gamma-ray efficiencies of long and short bursts indicate that the energy dissipation process of the prompt emission is most likely the same.

The energy release inferred for GRB 051221a can also be used to constrain the energy extraction mechanism, particularly in the context of merger models. Two primary mechanisms for energy extraction from the central engine have been discussed in the literature, namely $\nu\overline{\nu}$ annihilation or magnetohydrodynamic (MHD) processes, for example, the Blandford-Znajek process (e.g., Blandford & Znajek 1977; Lee et al. 2005b; Rosswog et al. 2003). Numerical simulations indicate that $\nu\overline{\nu}$ annihilation generally produces a less energetic outflow than MHD processes (Lee et al. 2005a). Rosswog & Ramirez-Ruiz (2002) show that even under the most favorable conditions, neutrino annihilation is unlikely to power a burst with a beaming-corrected energy in excess of few $\times 10^{48}$ ergs, while magnetic mechanisms can produce luminosities $\gtrsim 10^{52}$ ergs s^{-1} (Rosswog et al. 2003). Given that the beaming-corrected total energy for GRB 051221a is a factor of $\sim$10 larger than the predicted yield for the $\nu\overline{\nu}$ annihilation model, this may indicate that MHD processes are responsible.

We next compare the circumburst densities of long and short GRBs. In Figure 9 we show that the circumburst densities for short bursts cluster near $n \sim 10^{-2}$ cm^{-3}. On the other hand, the densities inferred for long GRBs range from about 10^{-2} to 10 cm^{-3} with a median value of about 2 cm^{-3}. The fact that the circumburst densities of short GRBs cluster at the low end of the distribution for long GRBs supports the notion that short bursts do not explode in rich stellar wind environments, but are instead consistent with interstellar densities.

Finally, we show that the host galaxy of GRB 051221a is actively forming stars at a rate of about 1.6 $M_\odot$ yr^{-1}, but at the same time exhibits evidence for an appreciable population of old stars ($\sim$1 Gyr). The inferred star formation rate is at least an order of magnitude larger than the values inferred for previous short GRB hosts and yet is at the low end of the distribution for long GRB hosts. Similarly, the inferred metallicity for the GRB 051221a host galaxy appears to be higher than those of long GRB hosts, indicating that it is more evolved. It is conceivable that the spread in short GRB host properties reflects a dispersion in the progenitor lifetimes such that the progenitor of GRB 051221a may be younger than those of GRBs 050509b and 050724, which occurred in elliptical galaxies (see also Prochaska et al. 2006; Gal-Yam et al. 2005). The potential spread in progenitor lifetimes may also be supported by the smaller offset of GRB 051221a compared to previous short bursts, but we caution that offsets are affected not only by progenitor lifetimes but also by the potential dispersion in kick velocities, host masses, and projection effects.

While the basic properties of short GRBs (redshifts, hosts, isotropic gamma-ray energies) are now available for several events, it is clear that detailed afterglow observations are required for a complete understanding of the burst properties. With the addition of GRB 051221a to the existing sample of only two well-studied events, we have embarked on a quantitative study of short bursts that over the next few years will shed light on the diversity of progenitors and energy extraction mechanisms.

The authors thank S. Rosswog for helpful discussions. As always, the authors thank Jochen Greiner for maintaining his GRB page. A. M. S. and S. B. C. are supported by the NASA Graduate Student Research Program. E. B. is supported by NASA through Hubble Fellowship grant HST-HF-01171.01 awarded by the STScI, which is operated by the Association of Universities for Research in Astronomy, Inc., for NASA, under

contract NAS 5-26555. A. G. acknowledges support by NASA through Hubble Fellowship grant HST-HF-01158.01-A awarded by STScI. K. R. is supported by the Gemini Observatory, which provided observations presented in this paper, and which is operated by the Association of Universities for Research in Astronomy, Inc., under a cooperative agreement with the NSF on behalf of the Gemini partnership: the National Science Foundation (United States), the Particle Physics and Astronomy Research Council (United Kingdom), the National Research Council (Canada), CONICYT (Chile), the Australian Research Council (Australia), CNPq (Brazil), and CONICET (Argentina). GRB research at Caltech is supported through NASA.

REFERENCES

Alard, C. 2000, A&AS, 144, 363
Aloy, M. A., Janka, H.-T., & Müller, E. 2005, A&A, 436, 273
Barthelmy, S. D., et al. 2005, Nature, 438, 994
Belczynski, K., Bulik, T., & Kalogera, V. 2002, ApJ, 571, L147
Berger, E., Kulkarni, S. R., & Frail, D. A. 2003a, ApJ, 590, 379
Berger, E., et al. 2003b, Nature, 426, 154
———. 2005, Nature, 438, 988
Blandford, R. D., & Znajek, R. L. 1977, MNRAS, 179, 433
Bloom, J. S. 2005a, GCN Circ., 4367, 1
———. 2005b, GCN Circ., 4368, 1
Bloom, J. S., Frail, D. A., & Kulkarni, S. R. 2003, ApJ, 594, 674
Bloom, J. S., et al. 2006, ApJ, 638, 354
Burrows, D., et al. 2006, ApJ, submitted (astro-ph/0604320)
Christensen, L., Hjorth, J., & Gorosabel, J. 2004, A&A, 425, 913
Cummings, J., et al. 2005, GCN Circ., 4365, 1
Cutler, C., & Thorne, K. S. 2002, preprint (gr-qc/0204090)
Dressler, A., Smail, I., Poggianti, B. M., Butcher, H., Couch, W. J., Ellis, R. S., & Oemler, A. J. 1999, ApJS, 122, 51
Eichler, D., Livio, M., Piran, T., & Schramm, D. N. 1989, Nature, 340, 126
Endo, Y., et al. 2005, GCN Circ., 4393, 1
Foley, R. J., et al. 2003, PASP, 115, 1220
Fox, D. B., et al. 2005, Nature, 437, 845
Fryer, C. L., Woosley, S. E., & Hartmann, D. H. 1999a, ApJ, 526, 152
Fryer, C. L., et al. 1999b, ApJ, 516, 892
Galama, T. J., et al. 1998, Nature, 395, 670
Gal-Yam, A., et al. 2005, ApJ, submitted (astro-ph/0509891)
Gehrels, N., et al. 2005, Nature, 437, 851
Ghirlanda, G., Ghisellini, G., & Lazzati, D. 2004, ApJ, 616, 331
Golenetskii, G., Aptekar, R., Mazets, E., Pal'shin, V., Frederiks, D., & Cline, T. 2005, GCN Circ., 4394, 1
Granot, J., & Sari, R. 2002, ApJ, 568, 820
Grupe, D., et al. 2006, ApJ, submitted (astro-ph/0603773)
Guetta, D., & Piran, T. 2005, A&A, 435, 421
Hjorth, J., et al. 2005a, ApJ, 630, L117
———. 2005b, Nature, 437, 859
Katz, J. I., & Canel, L. M. 1996, ApJ, 471, 915
Kelson, D. D. 2003, PASP, 115, 688
Kennicutt, R. C. 1998, ARA&A, 36, 189
Kulkarni, S. R. 2005, preprint (astro-ph/0510256)
Lee, W. H., Ramirez-Ruiz, E., & Granot, J. 2005a, ApJ, 630, L165
Lee, W. H., Ramirez-Ruiz, E., & Page, D. 2005b, ApJ, 632, 421
Li, L.-X., & Paczyński, B. 1998, ApJ, 507, L59
MacFadyen, A. I., Ramirez-Ruiz, E., & Zhang, W. 2005, preprint (astro-ph/0510192)
Mazzali, P. A., et al. 2002, ApJ, 572, L61
McGaugh, S. S. 1991, ApJ, 380, 140
McKenzie, E. H., & Schaefer, B. E. 1999, PASP, 111, 964
Nakar, E., Gal-Yam, A., & Fox, D. B. 2006, ApJ, 650, 281
Narayan, R., Paczynski, B., & Piran, T. 1992, ApJ, 395, L83
Norris, J., Sakamoto, T., Band, D., & Barthelmy, S. 2005, GCN Circ., 4388, 1
Osterbrock, D. E. 1989, Astrophysics of Gaseous Nebulae and Active Galactic Nuclei (Mill Valley, CA: Univ. Science Books)
Panaitescu, A. 2006, MNRAS, 367, L42
Panaitescu, A., & Kumar, P. 2002, ApJ, 571, 779
Parsons, A., et al. 2005, GCN Circ., 4363, 1
Peng, C. Y., Ho, L. C., Impey, C. D., & Rix, H.-W. 2002, AJ, 124, 266
Perna, R., Armitage, P. J., & Zhang, B. 2006, ApJ, 636, L29
Piran, T. 1999, Phys. Rep., 314, 575
Predehl, P., & Schmitt, J. H. M. M. 1995, A&A, 293, 889
Prochaska, J. X., et al. 2004, ApJ, 611, 200
———. 2006, ApJ, 642, 989
Richmond, M. W., et al. 1996, AJ, 111, 327
Rose, J. A. 1985, AJ, 90, 1927
Rosswog, S., & Ramirez-Ruiz, E. 2002, MNRAS, 336, L7
Rosswog, S., Ramirez-Ruiz, E., & Davies, M. B. 2003, MNRAS, 345, 1077
Sari, R., & Mészáros, P. 2000, ApJ, 535, L33
Sari, R., & Piran, T. 1999, ApJ, 517, L109
Sari, R., Piran, T., & Halpern, J. P. 1999, ApJ, 519, L17
Sari, R., Piran, T., & Narayan, R. 1998, ApJ, 497, L17
Sazonov, S. Y., Lutovinov, A. A., & Sunyaev, R. A. 2004, Nature, 430, 646
Schlegel, D. J., Finkbeiner, D. P., & Davis, M. 1998, ApJ, 500, 525
Smith, J. A., et al. 2002, AJ, 123, 2121
Soderberg, A. M., Nakar, E., Berger, E., & Kulkarni, S. R. 2006a, ApJ, 638, 930
Soderberg, A. M., et al. 2004, Nature, 430, 648
———. 2005, ApJ, 627, 877
———. 2006b, Nature, 442, 1014
van der Horst, A. J. 2005, GCN Circ., 4385, 1
Villasenor, J. S., et al. 2005, Nature, 437, 855
Wainwright, C., Berger, E., & Penprase, B. E. 2006, ApJ, submitted
Wren, J., Vestrand, W. T., White, R., Wozniak, P., & Evans, S. 2005, GCN Circ., 4380, 1
Yi, I., & Blackman, E. G. 1998, ApJ, 494, L163
Yost, S. A., Harrison, F. A., Sari, R., & Frail, D. A. 2003, ApJ, 597, 459
Zhang, W., Woosley, S., & MacFadyen, A. 2003, ApJ, 586, 356